Meandering: field experiments, laboratory experiments and numerical modeling

K. Blanckaert
ENAC, Ecole Polytechnique Fédérale, CH-1015 Lausanne, Switzerland and Faculty of Civil Engineering and Geosciences, Delft University of Technology, Delft, The Netherlands. Email: koen.blanckaert@epfl.ch, Phone: +41/21/6932378.

I. Schnauder and A. Sukhodolov
Department of Ecohydrology, Institute of Freshwater Ecology and Inland Fisheries, Berlin, Germany

W. van Balen and W.S.J. Uijttewaal
Faculty of Civil Engineering and Geosciences, Delft University of Technology, Delft, The Netherlands.

ABSTRACT: Preliminary results on meandering from field experiments, laboratory experiments and numerical modeling are reported. Field and laboratory measurements point to the important interaction between the flow and the bathymetry. The flow (re)distribution seems to be strongly determined by the bathymetry, and the outer bank configuration seems to interact with a rather wide flow region adjacent to the bank. 3D numerical simulations with LES and RANS codes indicate that turbulence plays a dominant role in configurations with flat bed, whereas the hydrodynamics in configurations with mobile-bed are dominated by the influence of the bathymetry. The simulations suggest that dunes have an effect of dominant magnitude on the hydrodynamics. They identify the description of sediment transport as the principal weak point in morphodynamic models. 1D hydrodynamic models capture the overall velocity distribution in sharp bends and clearly reveal and parameterize the underlying mechanisms.

1 INTRODUCTION

River meanders are major features on the Earth surface, which are characterized by shallows at the inside and deep scour holes at the outside of bends. The zone with maximum flow depth, called pool, and the maximum bend scour in the pool are the major parameters with respect to erosion at the outer bank and meander migration. The submergence of the zone of minimum flow depth, called point bar or riffle, varies with the flow stage, giving rise to spatio-temporal variations in flow and sedimentologic characteristics that makes it a hotspot for biodiversity. Developing vegetation at low flow stages stabilizes the point bar and plays an important role in accretion at the inner bank. Meander migration continuously reshapes the land and rejuvenates the floodplain. The highly dynamical character of meanders poses practical problems: bank erosion endangers property and leads to loss of fertile soil, the loss/gain of land at the outer/inner bank and the shifting boundaries are a legal concern, the variable depth and width complicate navigation, the continuous reworking of the meander belt leads to a heterogeneous sediment stratigraphy that complicates the exploitation of drinking water or hydrocarburates. But the dynamical meander belt offers an important retention capacity during flood events and it is a landscape element of great ecological value that offers a high potential for river restoration and revitalization. It is a challenge in river management and engineering to conciliate these threats and opportunities.

Since the seminal works of Fargue (1868), Boussinesq (1868) and Thomson (1876), meanders have continued to intrigue scientists and practitioners. In spite of the abundant research on all aspects of meandering rivers, insight in the relevant meander processes is still incomplete and the available engineering and management tools and models are characterized by uncomfortable uncertainties. The present paper focuses on the hydrodynamics in meandering rivers, whose accurate description is a prerequisite for progress in the understanding and modeling of transport, morphological and ecological processes.

The present paper's objective is to illustrate and report some preliminary results from joint research by Ecole Polytechnique Fédérale Lausanne (EPFL, Switzerland), Delft University of Technology (TUD, The Netherlands) and the Leibniz Institute of Freshwater Ecology and Inland Fisheries (IGB, Germany) that combines field experiments, laboratory experiments and numerical modeling. Results will be illustrated for a bend on the meandering Ledra River in the Friulian Alps, Italy, and a bend in a laboratory flume.

The investigated field and laboratory experiments will be reported in sections 2 and 3, respectively, whereas 3D and 1D numerical models will be discussed in section 4.The main results are discussed and summarized in section 5.

2 FIELD EXPERIMENT ON THE MEANDERING LEDRA RIVER

Research on natural meander bends has evolved in line with technological developments. The first research on natural meander bends by Fargue (1868) and Thomson (1876) was mainly based on observations. Rozovskii (1957) reported measured patterns of the horizontal and transverse velocity components, measured on rough grids. Dietrich and Smith (1983), Nelson and Smith (1989), Dietrich and Whiting (1989) investigated the flow and bed topography in a bend on Muddy Creek by means of a two-dimensional electromagnetic flow meter. A similar instrument was used by de Vriend and Geldof (1983) on the Dommel River and by Hodskinson and Ferguson (1998) on the Dean River. Ferguson et al. (2003) and Frottingham and Rhoads (2003) reported three-dimensional velocity measurements by means of Acoustic Doppler Velocimeters (ADV).

This section reports preliminary results from a recent measuring campaign in the spring of 2009 on a bend on the Ledra River (Figure 1), carried out by applying simultaneously three Nortkek ADV's. IGB conceived the experimental set-up and provided the instruments and logistics of this field campaign that was coordinated by A. Sukhodolov.

The Ledra River is a meandering tributary of the Tagliamento River in the Friulian alps. It is heavily canalized, except for the last kilometers upstream of its confluence with the Tagliamento, where the measurements took place. Flow depth and discharge in the Ledra varied by less than 5% during the measuring campaign, allowing for field measurements with an unprecedented spatial resolution on grids with more than 500 measuring points per cross-section. Six cross-sections have been measured in detail in the bend illustrated in Figure 1. The investigated reach has a nearly constant width of about 15m, an overall-averaged flow depth of about 1.5m, and a discharge of about 18 m^3s^{-1}. Flow is subcritical with a Froude number of about 0.3. The river is relatively narrow with an aspect ratio of about 10 and rather strongly curved with a ratio $R_{max}/B = 3$, where R_{max} is the centerline radius of curvature in the apex.

The bends at the beginning and end of the investigated reach are characterized by a typical point bar-pool bathymetry. The bend that has been measured in detail, on the contrary, has a rather surprising bathymetry (cf. Figures 1 and 3). There is no quasi-horizontal point bar at the inside of the bend, but rather a gradual increase of the flow depth from the inner bank towards about the middle of the cross-section where the maximum flow depth is situated. The flow depth is about constant in the outer half of the cross-section. The zone with quasi-constant flow depth seems to widen in streamwise direction. The streamwise evolution of the maximum scour depth and transverse bed slope are not typical either: they are not characterized by an overshoot in the beginning of the bend and a subsequent evolution towards an equilibrium value according to a damped oscillation as often observed in laboratory flumes and predicted by models of de Vriend and Struiksma (1984), Struiksma et al. (1985), Odgaard 1986), but increase gradually in the first half of the bend, reach their maximum around the apex, and subsequently decrease gradually again in the second part of the bend. Near the bend exit, there seems to be a local increase in scour depth and transverse bed slope.

The outer bank is steep (Figure 3) and characterized by a very irregular pattern due to the presence of trees, trunks and vegetation, local bank erosion, and small embayments. This irregular outer bank acts as a kind of macro-roughness and creates complicated near-bank flow patterns, such as horizontal recirculation zones.

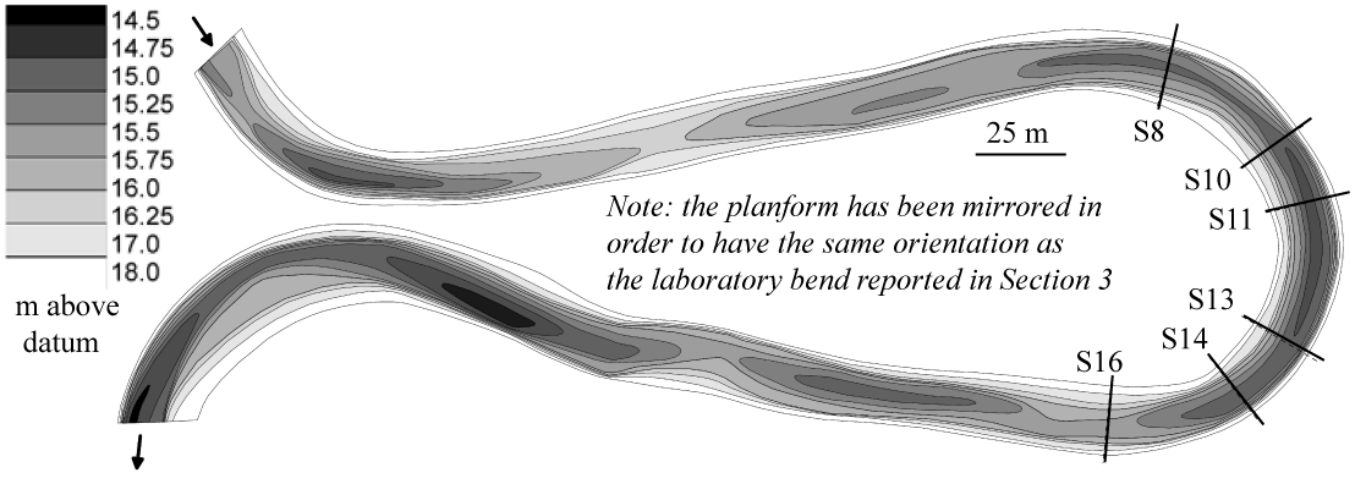

Figure 1. Planform and bathymetry of the meandering Ledra River (Courtesy A.Sukhodolov).

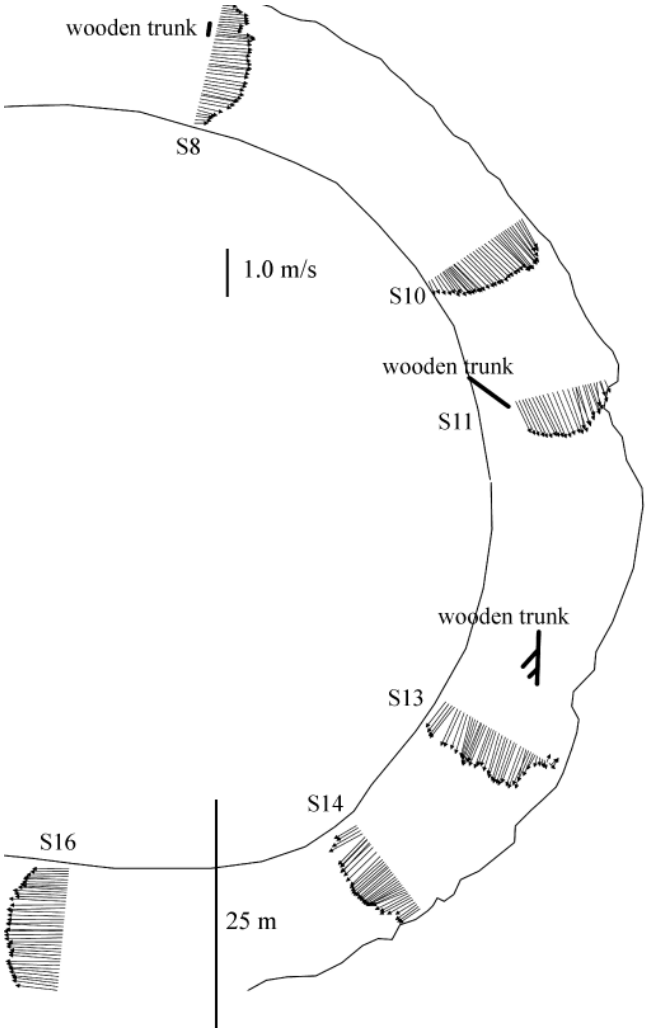

Figure 2: Depth-averaged velocity vectors (U_s,U_n) measured in the Ledra meander bend (Courtesy I. Schnauder)

Figure 2 illustrates the patterns of the depth-averaged velocity vectors (U_s,U_n), computed from measurements in about 30 vertical profiles with a vertical spacing of 0.1m between points. The velocity distribution is slightly inwards skewed in the cross-section S8 in the beginning of the bend. This may be due to the change in curvature, although also the influence of a trunk in the outer half of the cross-section may play a role. The velocity distribution is clearly outwards skewed in the cross-section S10, which requires outwards mass transport between S8 and S10. The core of maximum velocities seems to have shifted inwards in cross-section S11. The hydrodynamics in this cross-section are complicated, however, by the presence of a pronounced embayment at the outer bank and a large trunk floating at the water surface at the inner bank (Figure 2). Surprisingly, the velocities are nearly uniformly distributed over the width in the second part of the bend, which is related to the surprisingly flat bed in this part of the bend (cf. Figure 1). A slight outwards shift of the velocities seems to occur at the exit of the bend, which may be attributed to the decreasing curvature.

The pattern of streamwise velocities in the cross-section S10 are shown in Figure 3. Velocities are rather low over the shallow inner part of the cross-section, but characterized by a considerable transverse gradient. The velocities increase in outwards direction, but the core of maximum velocities stays at about 2m, corresponding to about once the local flow depth, from the outer bank. Vertical profiles of the velocities are rather flat in this region, and characterized by important near-bed gradients and a maximum value that occurs slightly below the water surface.

Figure 3 also shows the pattern of secondary flow, defined as the projection of the velocity vector in the cross-section. Inwards mass transport seems to occur over the entire flow depth close to the inner bank over the shallowest par of the cross-section. The typical curvature-induced secondary flow occurs in the central part of the cross-section. A counter-rotations outer-bank cell of secondary flow is discernable in the upper part of the flow depth adjacent to the outer bank. It occupies a zone with a width of about once the local flow depth. The core of maximum streamwise velocities seems to coincide with the separation between both secondary flow cells. In the same region, advection of flow towards the toe of the outer bank occurs, but it does not result in a discernable increase of near-toe streamwise velocities. The pattern of both secondary flow cells is very well reflected in the pattern of cross-sectional (transverse-vertical) shear stress.

The pattern of turbulent kinetic energy, *tke*, is visualized in Figure 3. In general, turbulence seems to be mainly dominated by bed friction, since it increases from the water surface towards the bed and increases in outwards direction in line with the distribution of the streamwise velocity. Turbulence levels seems to be slightly increased at the edges of the central cell of secondary flow, as well as in the region covered by the outer-bank cell of secondary flow. The highest levels of *tke* are found at the toe of the outer bank, where vertical velocities impinge on the bed. This may promote sediment transport and bank instability.

The patterns of the streamwise velocity, the secondary flow and the cross-sectional shear stress are similar to those observed by Blanckaert and Graf (2001) in a small laboratory flume with mobile bed. The mechanisms underlying the flow patterns will be further analyzed according to the methodology used by Blanckaert and Graf (2004) for the velocity (re)distribution, Blanckaert and de Vriend (2004) for the secondary flow and Blanckaert and de Vriend (2005a,b) for the turbulence characteristics.

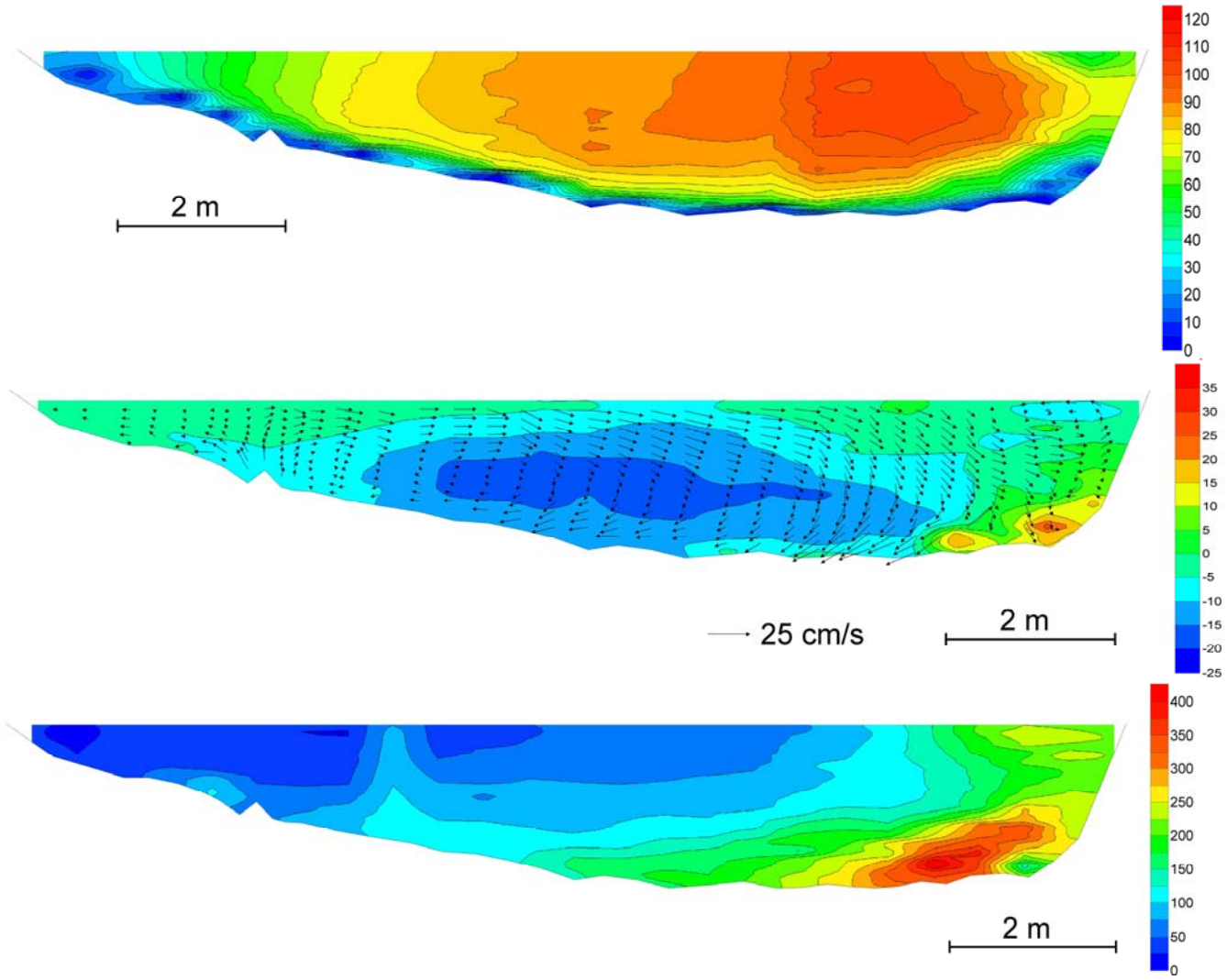

Figure 3. Patterns measured in the S10 cross-section (cf. Figures 1,2) on the Ledra meander bend: (top) Isoline pattern of the streamwise velocity, quantified by the colorbar in [cms^{-1}]; (middle) Vector pattern of secondary flow and isoline pattern of the transverse-vertical shear stress, quantified by the colorbar in [cm^{2}s^{-2}]; Isoline pattern of the turbulent kinetic energy, quantified by the colorbar in [cm^{2}s^{-2}]. (Courtesy I. Schnauder)

3 LABORATORY EXPERIMENTS

The laboratory environment provides a setting with controlled flow and boundary conditions defined with an accuracy exceeding that which could possibly be obtained in a field study. Moreover recent progress in instrumentation allowed measuring the bed and water surface topographies (acoustic limnimeters) and the 3D flow field (Acoustic Doppler Velocity Profiler) with unprecedented spatial and temporal resolution. Laboratory investigations concerning the bed topography have often been carried out with small flow depths (Whiting and Dietrich 1993), or under dynamic conditions with migrating bedforms (Abad and Garcia 2009) that did not allow for detailed velocity measurements whereas investigations of the flow field have often been carried out over schematized bed topographies (Yen and Yen 1971, de Vriend and Koch 1978). Laboratory investigations including detailed measurements of the flow and the bed topography are extremely scarce (Hooke 1974, Kikkawa et al. 1976, Odgaard and Bergs 1988) and concern weakly to moderately curved bends.

The reported experiments were carried out in the laboratory flume shown in Figure 4, which consists of a 193° bend of constant centerline radius of curvature, R = 1.7m, preceded by a 9m long straight inflow reach and a 5m long straight outflow reach. The width was constant at B = 1.3m. Experiments have been carried out over a mobile sand bed and over a fixed horizontal sand bed, with sand of mean diameter d = 2 mm. Geometric and hydraulic parameters of the experiments are summarized in Table 1.

Table 1. Geometric and hydraulic parameters in the laboratory experiments.

Experiment	Q	U	H	Fr	R/B	B/H
	[l/s]	[m/s]	[m]	[-]	[-]	[-]
Mobile bed	89	0.49	0.141	0.41	1.31	9.2
Horizontal bed	89	0.43	0.159	0.35	1.31	8.2

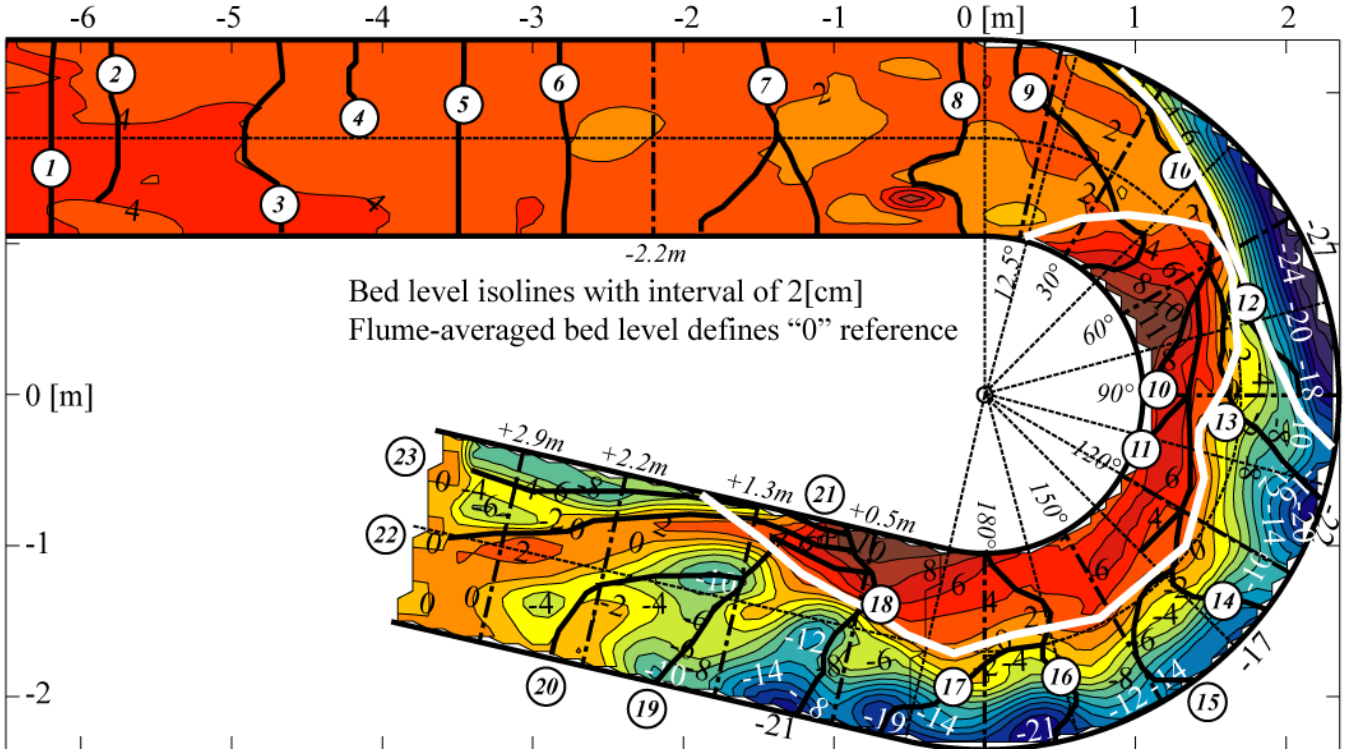

Figure 4. Isolines of the bed level with an interval of 0.02m derived from acoustic limnimeter measurements. Additional ADVP measurement with higher spatial resolution are available in the indicated cross-sections. The position of dunes is based on photographs. The flume-averaged bed level defines the reference level. The white lines delineate approximatively the point bar and pool. (bottom).

The Froude number and aspect ratio in the experiments are comparable to those in the Ledra meander bend. The curvature in the laboratory bend is considerably stronger as indicated by the ratio R/B.

Only the major results are reported in the present section; a more detailed presentation and analysis of the laboratory experiments is reported in Blanckaert (2009a, b).

The reported mobile-bed experiment started from an initial flat bed. Sediment was continuously fed at the flume entrance, resulting in bed-load sediment transport, such that a bathymetry developed that was in equilibrium with the flow. Once a state of dynamic equilibrium was reached, characterized by migrating dunes superimposed on the steady macro features of the bathymetry, sediment supply was stopped and the bathymetry was frozen by spraying paint on it that preserves the roughness, to enable detailed velocity measurements.

The frozen bathymetry (Figure 4) is characterized by a transverse bed slope that evolves as a damped oscillation towards an equilibrium value and overshoots this equilibrium value in the first part of the bend, whereby the maximum flow depth is about three times higher than the average flow depth. Such behavior has been explained and modeled by de Vriend and Struiksma (1984), Struiksma et al. (1985), Odgaard 1986), etc. Important bathymetric features include the pronounced quasi-horizontal point bar and pool in the inner/outer half of the cross-section in the first part of the bend, accompanied by quasi bi-linear transverse bed profiles. The cross-sectional shape is about linear in the second part of the bend. As compared to the Ledra bend, the bathymetry in the laboratory experiment shows more pronounced spatial variations and more pronounced transverse slopes.

Figure 5 shows the distribution around the flume of the normalized depth-averaged streamwise velocity. U_s/U. Moreover, it illustrates the location of the first moment (center of gravity) of the $U_s h$ pattern as well as the vector $\left(\langle\langle U_s h\rangle\rangle, \langle\langle U_n h\rangle\rangle\right)$ ($\langle\langle\ \rangle\rangle$ represents cross-sectional averaged values). Similar to the Ledra bend, the maximum velocities are not systematically found over the deepest part of the cross-section. A potential vortex velocity distribution establishes just downstream of the bend entry with maximum values near the inner bank. The maximum velocities are subsequently found over the pool which requires strong outwards mass transport. The maximum value of $U_n h/UH \approx 0.7$ indicates that the flow seems to go straight on and to collide with the outer bank at an oblique angle at about 60° in the bend. A horizontal recirculation zone is observed over the shallow point bar, similar to recirculation zones observed in natural rivers (Leeder and Bridge 1975, Frothingham and Rhoads 2003, Ferguson et al. 2003).

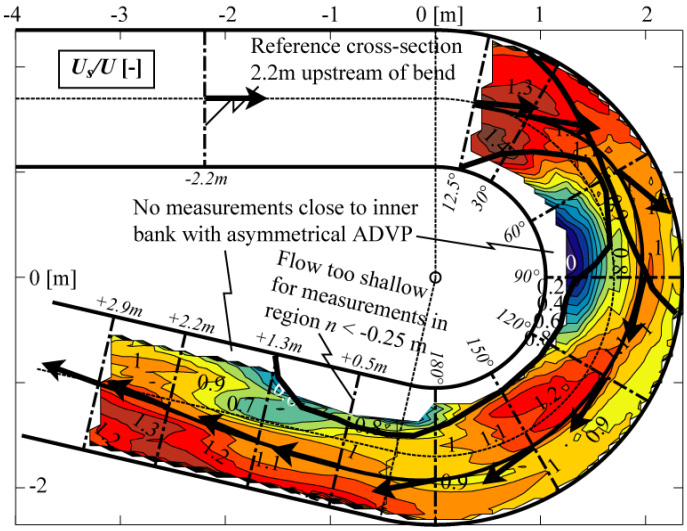

Figure 5: Normalized depth-averaged streamwise velocity, U_s/U [-]. Isoline pattern based on high-resolution measurements in the indicated cross-sections. The black lines delineate approximatively the point bar and pool. The black line with vectors indicates the first moment of the distribution of $U_s h/UH$, and the vectors $\left(\langle\langle U_s h\rangle\rangle, \langle\langle U_n h\rangle\rangle\right)/UH$.

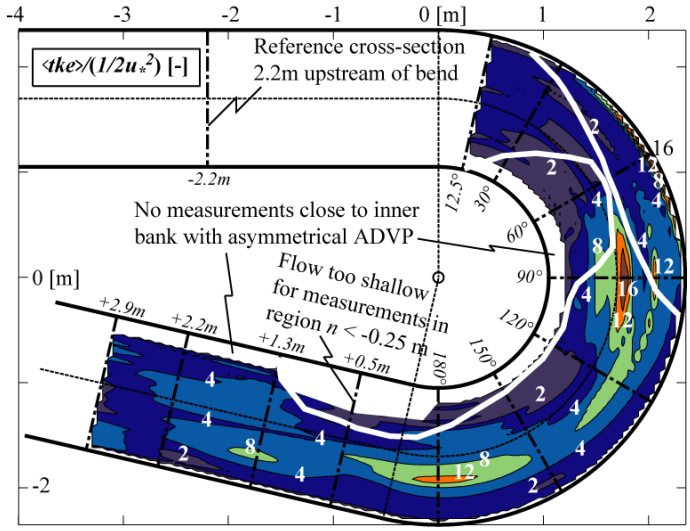

Figure 6: Isolines of normalized depth-averaged turbulent kinetic energy, $\langle tke\rangle/\left(1/2u_*^2\right)$ [-]. Patterns are based on high-resolution measurements in the indicated cross-sections. The white lines delineate approximatively the point bar and pool.

Flow does not separate at the bend entry, but only at about 40 ° in the bend, which can be attributed to the discontinuity in curvature at the bend entrance that leads to pronounced local accelerations/decelerations in the inner/outer-half of the cross-section and corresponding inwards mass transport that opposes flow separation. Therefore, this is rather an artifact of the specific laboratory configuration that is not representative of flow separation in natural river meanders. The flow recirculation zone reaches its maximum width in the cross-section at 80°, where it spans about 2/3 of the total width.

The maximum velocities move again inwards downstream of the cross-section at 90°, accompanied by inwards mass transport. A pronounced outwards shift of the maximum velocity occurs at the bend exit, with corresponding strong flow deceleration over the shallow at the inside of the bend. Velocities tend to uniformise in the straight outflow reach.

The transverse mass flux, $U_n h$, behaves like a damped oscillation in streamwise direction, in close relation to the damped oscillation of the transverse bed slope (Figure 4), as explained and quantified by models of de Vriend and Struiksma (1984), Struiksma et al. (1985), Odgaard 1986). The pattern of depth-averaged streamwise velocities (Figure 5), leaves a clear footprint on the observed dune pattern (indicated in Figure 4), which is representative for the migration speed of the dunes and the related sediment transport rate. The overall features of the depth-averaged velocity pattern in the Ledra bend (Figure 2) and the laboratory bend (Figure 5) are quite similar. Gradients are more pronounced in the latter, however, which may be due to the more pronounced curvature.

Blanckaert (2009b) has made a detailed analysis of the mechanism underlying the velocity redistribution by means of a term-by-term analysis of the depth-averaged momentum equation.

The distribution of the normalized depth-averaged turbulent kinetic energy, $\langle tke\rangle/\left(1/2u\right)_*^2$, which plays an important role with respect to sediment transport, mixing and spreading of oxygen, nutrients, pollutants, heat, etc, is shown in Figure 6. The background value of about 4 characterizes bed generated turbulence in agreement with Nezu and Nakagawa's (1993) semi-theoretical profiles in straight open-channel flow. The turbulence activity does not show a dominant signature of the bed topography since the maximum turbulence activity is not found over the deepest parts of the cross-sections. Different physical processes locally increase the turbulence activity (see Blanckaert 2009b). The flow colliding with the bank and additional shear by the strong secondary flow locally increase the turbulence activity over the deepest part of the pool in the bend region between 30° and 90°. Additional shear by the weaker curvature-induced secondary flow downstream of the cross-section at 120° in the bend also considerably increases the turbulence activity. Blanckaert (2009a) has modeled the generation of turbulent kinetic energy by the curvature-induced secondary flow, which will not further be considered here. Horizontal shear due to transverse gradients in U_s and $U_s h$ increases the turbulence activity near the centerline downstream of the cross-section at 60° and slightly outwards of the centerline downstream of the cross-section at 150°. The turbulence activity over the point bar seems to be reduced.

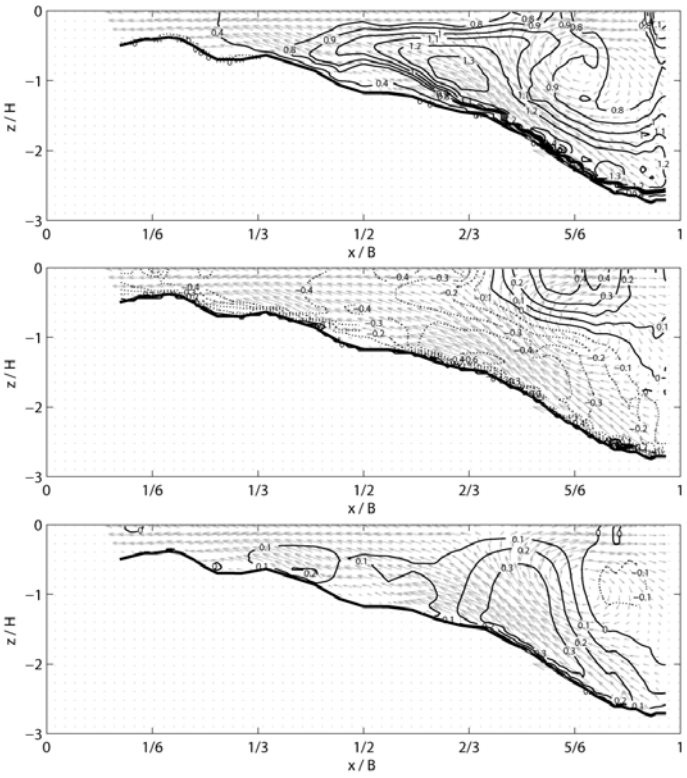

Figure 7: Patterns of the measured normalized streamwise (top), transverse (middle) and vertical (bottom) velocities in the cross-section at 90° in the bend (Courtesy W. van Balen).

Obviously, three-dimensional flow structures, such as secondary flow, play an essential hydrodynamic role. Figure 7 shows the patterns of normalized streamwise, transverse and vertical velocities in the cross-section at 90° in the bend. This cross-section is situated at the downstream end of the point bar – pool zone in a region characterized by inwards mass transport (Figure 5). The bed in this cross-section is about flat in the inner third of the cross-section occupied by the point bar and about linear in the pool.

The curvature-induced secondary flow is limited to the outer-half of the cross-section, whereas inwards mass transport occurs over the point bar. Maximum transverse velocities in both zones reach considerable magnitudes of $v_n/U = 0.4$. Maximum upwelling and downwelling vertical velocities are about $v_z/U = +0.3$ and -0.1, respectively. The positive skewing of the vertical velocities is due to the presence of a dune (cf. Figure 4).

Secondary flow is commonly modeled and explained as resulting from the quasi-balance between the outwards centrifugal force and the inward pressure gradient due to the transverse tilting of the water surface. This oversimplified modeling is not adequate in the illustrated point bar-pool zone of the bend, where also inertia and advective momentum transport play an important role. The considerable downwelling velocities are responsible for the scouring of the bed in the pool. Due to mass conservation, the downwelling velocities impinging on the bed give rise to inwards transverse velocities, whose magnitude determines the transverse bed slope of the pool zone (Blanckaert 2009b).

Advective momentum transport by the secondary flow seems to have a dominant effect on the pattern of streamwise velocities. The strong downwelling velocities near the outer bank are responsible for the low near-surface velocities and the high near-bed velocities. The core of highest streamwise velocities is spread near the bed by the inwards transverse component of the secondary flow. These high near-bed velocities promote sediment transport and bend scour in the pool region. Streamwise velocities are considerably lower over the point bar, where relatively important transverse gradients occur.

The experiments in the Ledra River and the laboratory experiment have highlighted the importance of the flow patterns near the outer bank and their interaction with the outer-bank geometry. The influence of the inclination and roughness of the outer bank has been investigated in a series of nine laboratory experiments over fixed horizontal sand bed, covering three different bank inclinations (30°, 45° and 90°) and three different roughness characteristics (smooth, the same sand roughness as the bed and riprap with a equivalent roughness of k_s = 30 mm) by Duarte (2008). The experiments were carried out with similar overall flow depth and velocity (cf. Table 1).

Additional cells of secondary flow, called outer-bank cells, have been observed long ago in the laboratory (e.g. Mockmore 1943, Einstein and Harder 1954, Rozovskii 1957) and in the field (e.g. Bathurst, Thorne and Hey 1977, 1979, Thorne and Hey 1979, Thorne et al. 1985). Recently, Blanckaert and Graf (2004) and Blanckaert and de Vriend (2004) have carried out detailed measurements of an outer-bank cell in a smaller laboratory flume with vertical banks by means of the same instruments used in the here presented experiments.

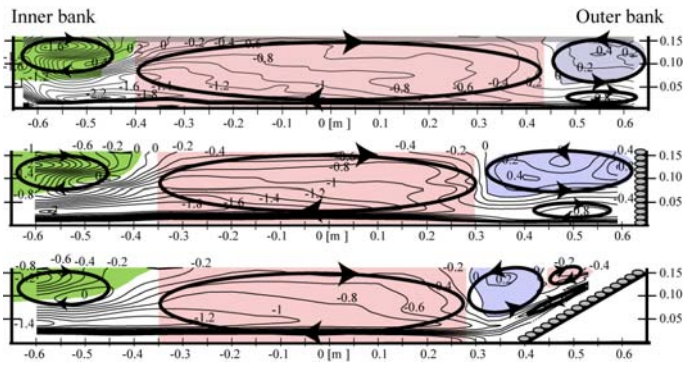

Figure 8. Measured patterns of the secondary flow, quantified by the normalized streamwise component of the vorticity, $\omega_s H/U$ in experiments with fixed horizontal bed and smooth vertical outer bank (top), riprap-roughened vertical outer bank (middle) and riprap-roughened outer bank inclined at 30° (bottom).

The outer-bank cells are known to be relevant with respect to the stability of the outer bank and the adjacent bed. According to Bathurst, Thorne and Hey (1979) they endanger bank stability, whereas Blanckaert and Graf (2004) pretend that they protect the outer bank and the adjacent bed by forming a buffer layer that protects the outer bank and adjacent bed from any influence of the center-region cell: the central secondary flow cell redistributes the velocity and causes it to increase towards the outer bank, whereas the outer-bank cell prevents this increase to continue through to the bank and keeps the core of maximum velocity a distance from the bank at the separation between both cells.

Figure 8 illustrates the measured patterns of the secondary flow in the cross-section at 90° in the bend in experiments with smooth vertical outer bank, rough vertical outer bank, and rough 30°-inclined vertical outer bank. The secondary flow is quantified by means of the streamwise component of the vorticity, defined as $\omega_s = \partial v_z/\partial n - \partial v_n/\partial z$. Contrary to the mobile-bed experiment, outer-bank cells occur under all investigated conditions in the horizontal bed experiments. An increase in outer-bank roughness seems to widen and strengthen considerably the outer-bank cell, whereas inclining the outer bank seems to weaken the outer-bank cell and to change its pattern. But its protective effect by forming a buffer layer between the outer bank and the center-region cell seems to be conserved. More details are reported in Duarte (2008), who analysis the mechanisms underlying the near-bank secondary flow cells by means of a term-by-term analysis of the vorticity equation and the kinetic energy fluxes between the mean flow and the turbulence, similar to Blanckaert and de Vriend (2004).

The hydrodynamic characteristics over horizontal and mobile bed bathymetries are fundamentally different, as indicated for example by the appearance of additional secondary flow cells near the inner bank over horizontal bed.

4 NUMERICAL MODELLING

4.1 *A 3D LES hydrodynamic model*

The 3D LES code reported by van Balen et al. (2009) simulates accurately the flow in a mildly curved laboratory bend with horizontal bed (van Balen, Uijttewaal and Blanckaert 2009), the here presented strongly curved laboratory flume with horizontal bed (van Balen, Blanckaert and Uijttewaal 2009) and the here presented strongly curved laboratory bend with mobile bed (Figure 9 vs. Figure 7).

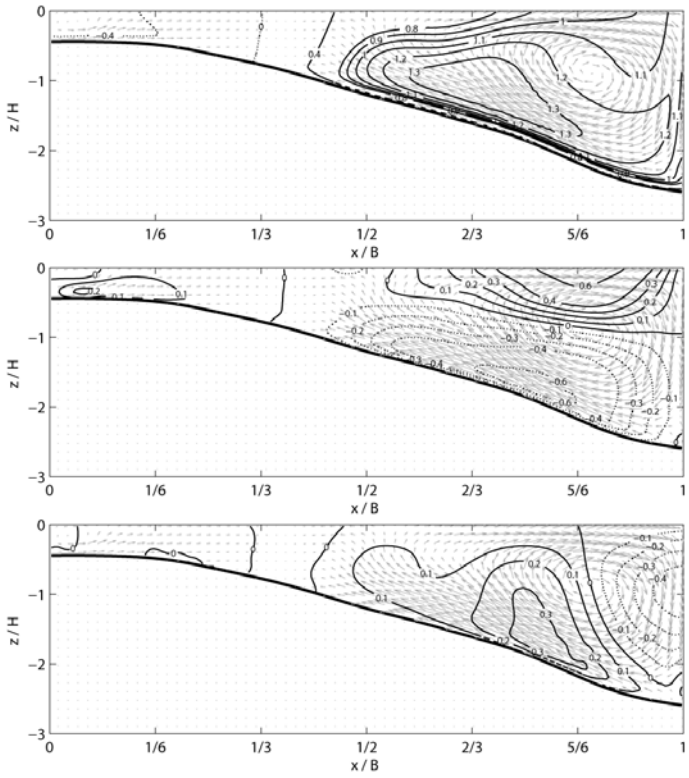

Figure 9: Patterns of the simulated normalized streamwise (top), transverse (middle) and vertical (bottom) velocities in the cross-section at 90° in the bend (Courtesy W. van Balen).

Considerable deviations occur, however, in the patterns of the streamwise and vertical velocities. These differences are mainly attributed to the neglect of the dunes (cf. Figure 4) in the simulations, indicating that the effect of the dunes on the hydrodynamics is of dominant order of magnitude.

The patterns of the normalized streamwise velocity v_s/U (Figure 10) and normalized turbulent kinetic energy tke/U^2 (Figure 11) around the bend indicate that the 3D LES model resolves accurately the velocity (re)distribution and the zone of flow recirculation over the point bar as well as the increase in turbulence activity generated by additional horizontal shear or secondary flow.

The results from the simulations allow gaining further insight in the meander hydrodynamics. Contrary to the experimental data, the simulated data are not limited by a low spatial resolution in streamwise direction or by experimental scatter and uncertainty. Hence they are particularly appropriate for term-by-term analyses of the flow equations. Van Balen et al. (2009a, b) have analyzed the mechanisms underlying the near-bank cells of secondary flow in a mildly curved laboratory bend with horizontal bed and the here presented strongly curved laboratory flume with horizontal bed, respectively, and highlighted the important role played by turbulence.

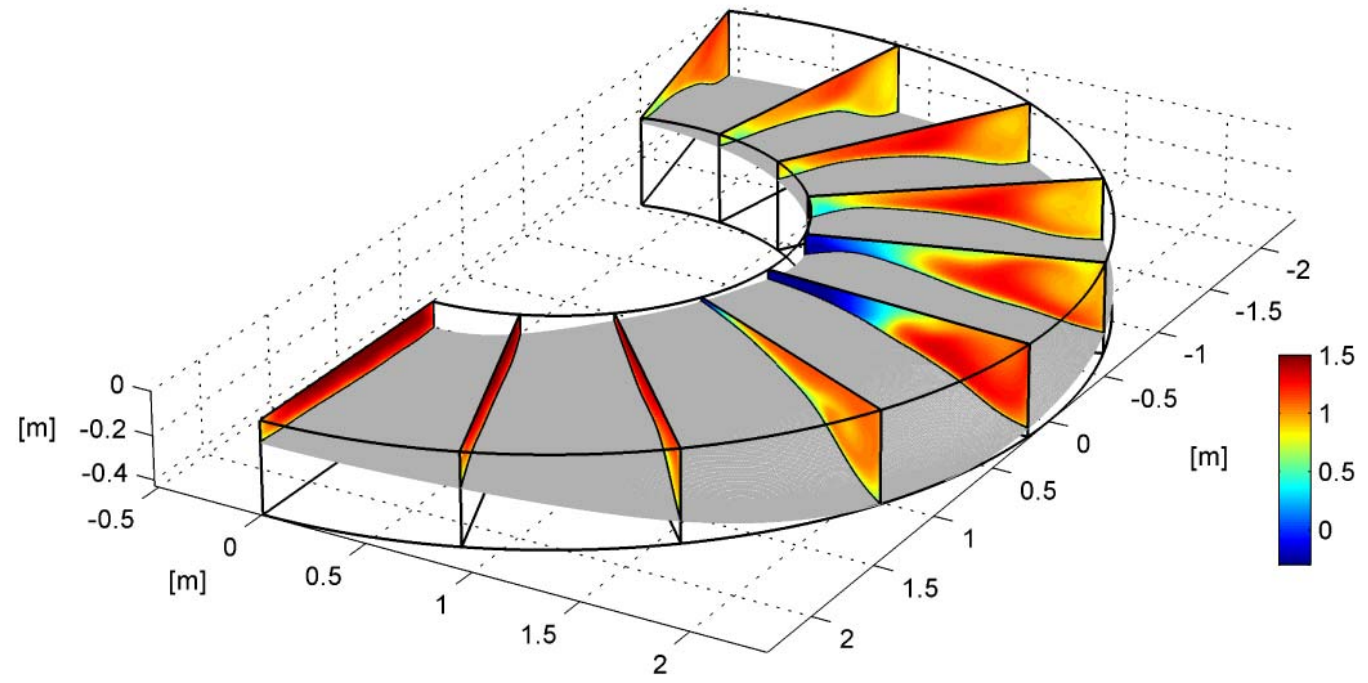

Figure 10. Patters of the normalized streamwise velocity, v_s/U computed by means of the 3D LES code. (Courtesy W. van Balen)

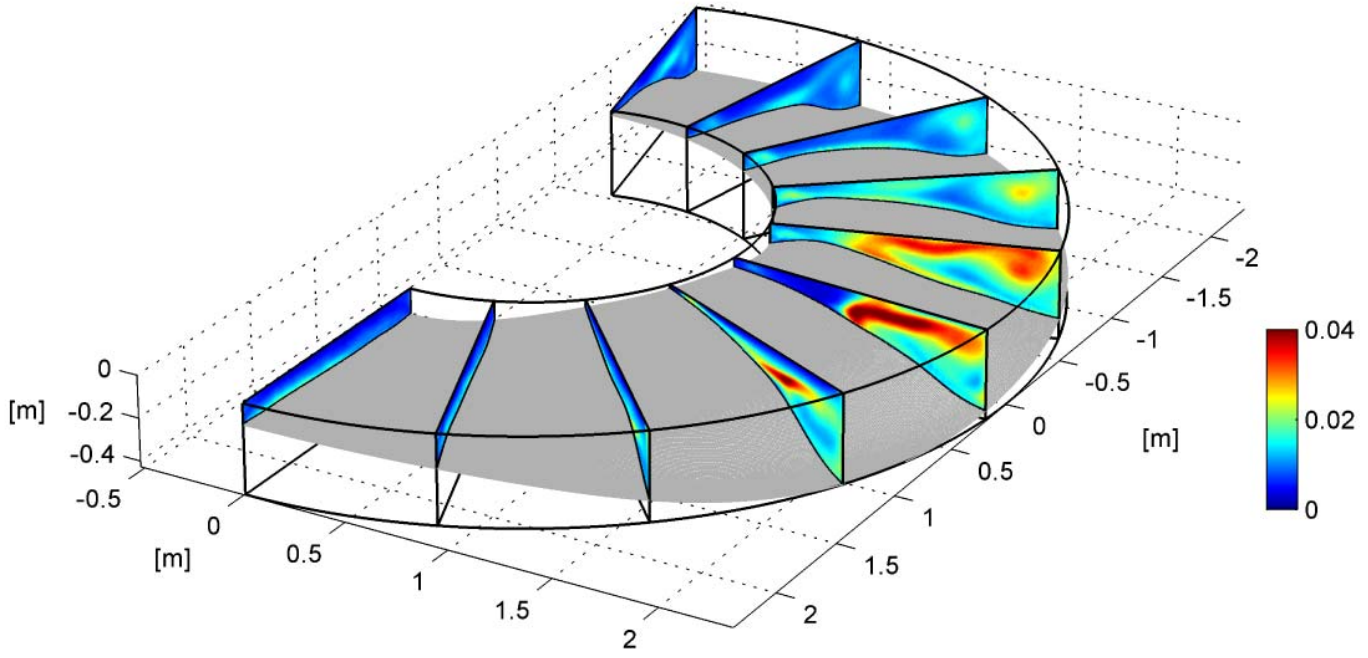

Figure 11. Patters of the normalized turbulent kinetic energy, tke/U^2 computed by means of the 3D LES code. (Courtesy W. van Balen)

The LES simulations also provide data in flow regions that are not accessible by the velocimeters, such as the flow regions close to the solid boundaries and the water surface, and variables that cannot easily be measured, such as the pressure distribution. Van Balen et al. (2009a, b), for example, investigate the shear stresses on the bed and the banks. Meander hydrodynamics are currently further investigated by means of the 3D LES code by reducing and enlarging the investigated parameter space. The former is done by considering so-called axisymmetric flow where the flow has completely adapted to curvature and no streamwise gradients occur. The latter is done by varying systematically one parameter, such as the width, roughness or curvature radius, while maintaining constant all other parameters.

4.2 *A 3D RANS morphodynamic model*

Zeng et al. (2008) have simulated the here reported horizontal and mobile-bed experiment by means of a 3D RANS morphodynamic code, with Spalart-Almaras turbulence closure.

The hydrodynamic simulations over prescribed mobile-bed bathymetry agreed very well with the 3D LES simulation. Contrary to the 3D LES simulations, the 3D RANS code was not able to resolve accurately the near-bank flow patterns, and especially the near-bank cells of secondary flow, over horizontal bed. These results indicate that the role of turbulence in natural configurations with mobile bed is less important than in artificial laboratory configurations with fixed horizontal bed.

When simulating the flow field and the bathymetry by means of the morphodynamic code, deviations between model predictions and measurements increased, but the main features were still captured by the model. This suggests that the main weakness in morphodynamic codes is related to the modeling of sediment transport. Commonly used models for sediment transport are based on formulations derived for straight uniform shear flows and are unable to account for hydrodynamic processes like downwelling vertical velocities impinging on the bed or increased turbulence activity near the bed.

4.3 *A 1D hydrodynamic model*

Despite the rapid evolution of computational power, one-dimensional (1D) modeling of meandering river flow and morphology can be expected to remain practically relevant, not only for rapid assessments, but also for probabilistic morphological predictions and basin-scale simulations of morphology and sediment deposit structures. Moreover, 1D models have the advantage of their simplicity and transparency.

Since the seminal models of Engelund (1974) and Ikeda, Parker and Sawai (1981), mathematical models of meander hydrodynamics and meander evolution have been continuously further developed and refined. Recent developments were mainly made by Seminara (2006), Camporeale et al. (2007), Crosato (2008, chapter 4) and Pittaluga et al. (2009), who summarize and compare existing 1D models for meander dynamics. All of these models are somehow based on the assumption of mild curvature. Blanckaert and de Vriend (2003, 2009) have proposed a 1D model for meander hydrodynamics that remains valid in the high curvature range and encompasses the mild-curvature model of Johannesson and Parker (1989).

Their model can formally be written in the form of a linear relaxation equation in the variable α_s that parameterizes the transverse distribution of the streamwise velocity, with adaptation length $\lambda_{\alpha s}/R$ and driving mechanism $F_{\alpha s}/R$:

$$\frac{\alpha_s}{R} = \left(1 + n/R\right)\frac{1}{U_s}\frac{\partial U_s}{\partial n} \tag{2}$$

$$\lambda_{\alpha s/R}\,\frac{\partial}{\partial s}\left(\frac{\alpha_s}{R}\right) + \frac{\alpha_s}{R} = F_{\alpha s/R} \tag{3}$$

$$\lambda_{\alpha s/R} = \frac{1}{2}\frac{H}{\psi C_f}\left\{1 - \frac{1}{12}\frac{\alpha_s + 1}{R}\frac{B^2}{R}\right\} \tag{4}$$

$$\begin{aligned} F_{\alpha s/R} = {} & \frac{1}{2}\frac{S_n Fr^2 + \mathrm{A} - 1}{R} \\ & - \frac{1}{2}\frac{H}{\psi C_f}\frac{\partial}{\partial s}\left(\frac{1}{R}\right)\left(1 - \frac{B^2}{6R^2}\right) \\ & + \frac{4\chi}{\psi C_f}\frac{H^2}{B^2}\frac{\langle f_s f_n\rangle}{R}\left[1 + \frac{1}{12}\frac{\left(S_n Fr^2 + \mathrm{A} + 3\right)B^2}{R^2}\right] \\ & + \frac{1}{24}\frac{H}{\psi C_f}\frac{B^2}{R^2}\frac{\partial}{\partial s}\left(\frac{S_n Fr^2 + \mathrm{A}}{R}\right) \end{aligned} \tag{5}$$

The coefficient ψ parameterizes curvature-induced energy losses and S_n is a coefficient of order 1. This equation clearly indicates the processes underlying the velocity redistribution. The first term (I) in Equation (5) represents the effect of the transverse slopes of the bed and the water surface, parameterized by the coefficient A and the Froude number, respectively. The second term (II) represents local flow accelerations/decelerations due to the adaption of the transverse water surface slope (superelevation) to changes in curvature. The third term (III) represents velocity redistribution by the secondary flow. It is parameterized by $\langle f_s f_n\rangle / R$, which is determined from the relation (see Blanckaert and de Vriend 2003):

$$\langle f_s f_n\rangle = fct\left(C_f\right).fct\left(C_f^{-0.275}\left(\frac{H}{R}\right)^{0.5}\left(\alpha_s + 1\right)^{0.25}\right) \tag{6}$$

The second functional relation in Equation (6) accounts for the non-linear interaction between the horizontal flow distribution (α_s) and the vertical flow distribution ($f_s f_n$). The fourth term (IV) represents velocity redistribution by the cross-flow U_n resulting from streamwise variations in the transverse slopes of the bed and the water surface. When assuming that B/R is small, $\psi \approx 1$, the coefficient χ=1.5, and the second functional relation in Equation (6) is identical to one, the model reduces to the widely used mild-curvature model of Johannesson and Parker (1989).

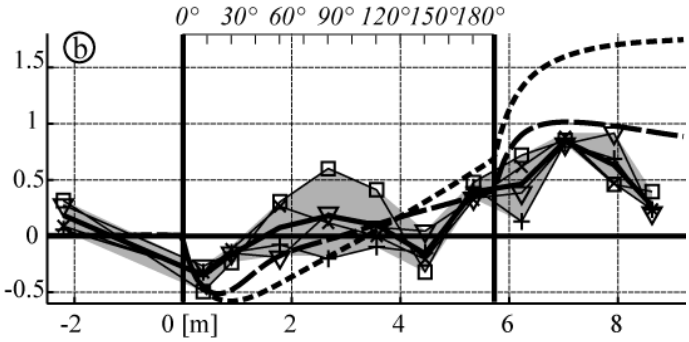

Figure 12: Evolution of α_s/R around the flume in the mobile-bed experiment obtained from: (i) the experimental data (labeled lines, full lines and gray area) (ii) the proposed 1D model without curvature restrictions (long-dashed line); (iii) the proposed model in its asymptotic formulation for mild curvature (short-dashed line).

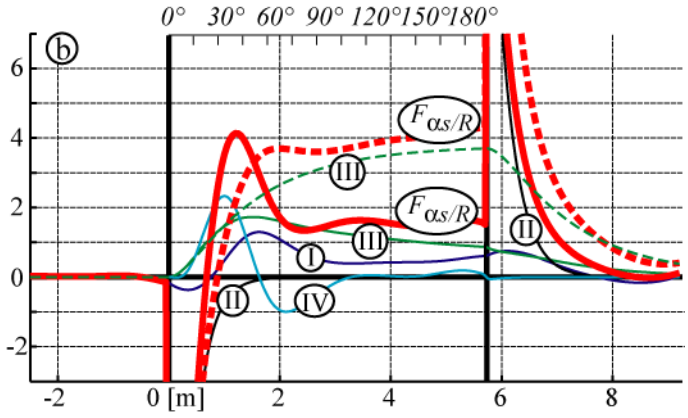

Figure 13: Evolution around the flume of the mechanisms that drive the velocity redistribution according to Equation (5) for the model without curvature restrictions (full lines) and the mild-curvature model (dashed lines). The labels on the curves correspond to the terms in Equation (5).

Figure 12 compares the evolution of α_s/R around the bend in the laboratory experiment with mobile bed, obtained from: (i) the experimental data; (ii) Blanckaert and de Vriend's 1D model without curvature restrictions; (iii) Blanckaert and de Vriend's 1D model in its asymptotic formulation for mild curvature. Obviously the complex 3D velocity pattern can only be parameterized by means of the single variable α_s/R (cf. Equation (2)) in an approximate way. Therefore, Figure 12 includes an uncertainty range (gray area) for the estimations from the experimental data. The mild curvature model significantly overestimates the outwards velocity distribution. Although significant deviations occur locally, the proposed model without curvature restrictions agrees globally satisfactorily with the data. Obviously a 1D description cannot capture all relevant hydrodynamic processes, which requires a 3D approach.

The transparency of the 1D model is exploited in Figure 13, which shows the evolution around the bend of the mechanism that drive the velocity redistribution according to Equation (5). According to the model, all four mechanisms are of dominant order of magnitude. Remarkably, variations in curvature (term II) are the dominant contribution. Differences between the model without curvature restrictions and the mild-curvature model are considerable and include: (i) a reduction of the effect of the secondary flow (term III) due to non-linear interactions between the horizontal and vertical structures of the flow; (ii) velocity redistribution due to streamwise changes in the bed and water surface topography (term IV) which are not accounted for in the mild-curvature model; (iii) reduction of the driving mechanisms due to the curvature-induced increase in energy losses parameterized by ψ (Terms II, III and IV).

The proposed model identifies $C_f^{-1}H/R$ as the main control parameter with respect to the velocity redistribution in curved open-channel flow. The driving mechanisms related to streamwise variations in curvature and the transverse bed and water surface slopes scale with it and the normalized adaptation length, $\lambda_{\alpha s/R}/R$ (cf. Equation (4)) is proportional to it.

de Vriend (1981) identified $C_f^{-1}H/R$ as an important control parameter with respect to the formation of an outer-bank cell of secondary circulation. Because it represents a ratio between forcing by curvature (H/R) and dissipation by boundary-friction generated turbulence (C_f), he called $C_f^{-1}H/R$ the Dean number, similar to its definition in curved laminar flow. Blanckaert and de Vriend (2003) identified $C_f^{-1}H/R$ as a major control parameter with respect to the vertical structure of the flow field and its interaction with the transverse flow structure. Johannesson and Parker (1989b) identified a similar parameter, $2\pi C_f^{-1}H/\lambda_m$ (λ_m is the meander wavelength), which they called the reduced wavenumber. The ratio B/R is traditionally the major scaling parameter used in field studies on meandering rivers. With respect to the velocity redistribution, B/R does not play a major role in mildly curved bends, but may be significant in sharp bends (cf. Equations (5)). The parameter set $C_f^{-1}H/B$ and B/R is equivalent to the parameter set $C_f^{-1}H/R$ and B/R. $C_f^{-1}H/B$ has the advantage that it characterizes a river reach and is independent of the curvature of individual bends.

5 DISCUSSION AND CONCLUSIONS

The present paper illustrated and reported some preliminary results from joint research by Ecole Polytechnique Fédérale Lausanne (Switzerland), Delft University of Technology (The Netherlands) and the Leibniz Institute of Freshwater Ecology and Inland Fisheries (Germany) that exploits synergies between field experiments, laboratory experiments and numerical modeling.

Three dimensional velocity measurements with high spatial and temporal resolution allowed identifying the relevant hydrodynamic processes in a bend on the Ledra River. The preliminary results indicate surprisingly uniformly distributed velocities in the second part of the bend, and a surprisingly small transverse inclination of the bed. The results furthermore indicate that the macro-roughness of the outer bank, formed by trees, protruding trunks, vegetation and small embayment, plays a major role with respect to hydrodynamics in a rather wide zone adjacent to the outer bank. These observations point to the importance of the interaction between the hydrodynamics, the sediment transport, the bathymetry and the ecology on a global scale as well as a very local scale.

The hydrodynamic processes observed in the Ledra meander bend were successfully reproduced in laboratory experiments under controlled conditions, which allowed for measurements with a higher spatial resolution and for the systematic investigation of the influence of individual parameters. Differences between the Ledra river and the laboratory flume can mainly be attributed to the more pronounced curvature in the laboratory bend. The interaction between the near-bank hydrodynamics and the configuration of the outer-bank has been investigated in horizontal bed experiments by systematically varying the roughness and inclination of the outer bank.

The hydrodynamics in the laboratory experiments have successfully been simulated by means of a 3D LES code. The simulated results were found to be appropriate for term-by-terms analysis of the flow equation thanks to their very high spatial resolution and lack of scatter, which allowed gaining insight in the mechanism underlying the near-bank flow patterns, and especially the outer-bank cells of secondary flow. The simulated results suggest that dunes have an effect of dominant magnitude on the hydrodynamics.

A 3D RANS code simulated successfully the hydrodynamics over a mobile bed, but performed considerably worse over a horizontal bed. This suggests that the structure of turbulence is of dominant importance in artificial configurations with horizontal bed, but not in natural river configurations where the influence of the bed topography is dominant.

Simulation of the morphodynamics considerably deteriorated the predictive capacities of the codes, suggesting that the major weakness of the morphodynamic code is related to the description of sediment transport, which does not account for hydrodynamic processes like downwelling vertical velocities impinging on the bed or increased turbulence activity near the bed.

A 1D hydrodynamic model is able to capture the overall velocity distribution in sharp bends, on the condition that it accounts for the non-linear interaction between the horizontal and vertical distributions of the flow. The reported 1D model for sharp bends clearly reveals and parameterizes the mechanisms underlying the velocity redistribution.

This research was supported by the Swiss National Science Foundation under grants 2100-052257.97 and 2000-059392.99, by Dutch Technology Foundation, applied science division of NWO under grants, DCB-6787 and DCB-7780 and by the Deutsche Forschungsgemeinschaft (DFG) and the Netherlands Organization for Scientific Research (NWO) under grants SU 405/3-1 and DN66-149 in the framework of their bilateral cooperation program.

REFERENCES

Abad, J. D., and M. H. Garcia (2009), Experiments in a high-amplitude Kinoshita meandering channel: 2. Implications of bend orientation on bed morphodynamics, Water Resour. Res., 45, W02402, doi:10.1029/2008WR007017.

Bathurst, J. C., Thorne, C. R., and Hey, R. D. (1977). "Direct measurements of secondary currents in river bends." Nature, 269, 504-506.

Bathurst, J. C., Thorne, C. R. and Hey, R. D. (1979). "Secondary flow and shear stress at river bends." J. Hydr. Div., ASCE, 105(10), 1277-1295.

Blanckaert, K. (2009a). "Saturation of curvature induced secondary flow, energy losses and turbulence in sharp open-channel bends. Laboratory experiments, analysis and modeling". Journal of Geophysical Research – Earth Surface (in press).

Blanckaert, K (2009b). " Topographic steering, flow recirculation, velocity redistribution and bed topography in sharp meander bends ". (submitted for publication to Water Resources Research - AGU). (Available on available on ftp://lrhmac17.epfl.ch/pub/Blanckaert/Blanckaert_WRR_2009/).

Blanckaert, K., and de Vriend, H. J. (2003). "Nonlinear modeling of mean flow redistribution in curved open channels." Water Resour. Res., 39(12), 1375–1388.

Blanckaert, K., and de Vriend, H. J. (2004). "Secondary flow in sharp open-channel bends." J. Fluid Mech., 498, 353–380.

Blanckaert, K. & de Vriend, H. J. (2005a). "Turbulence characteristics in sharp open-channel bends." Physics of Fluids, AIP, Vol. 17(5)-055102. (doi:10.1063/1.1886726)

Blanckaert, K. and de Vriend, H. J. (2005b). "Turbulence structure in sharp open-channel bends." Journal of Fluid Mechanics, Vol. 536, 27-48.

Blanckaert, K. and de Vriend H.J. (2009). "Meander dynamics: a 1D flow model without curvature restrictions" (submitted to Journal of Geophysical Research – Earth Surface; available on ftp://lrhmac17.epfl.ch/pub/Blanckaert/Blanckaert_JGR3_2009/)

Blanckaert, K., and Graf, W. H. (2001). "Experiments on flow in an open-channel bend. Mean flow and turbulence." J. Hydraul. Eng.,127(10), 835–847.

Blanckaert, K., and Graf, W. H. (2004). "Momentum transport in sharp open-channel bends." J. Hydraul. Eng., 130(3), 186–198.

Boussinesq, J. (1868). "Mémoire sur l'influence de frottement dans les mouvements réguliers des fluides; XII - Essai sur le mouvement permanent d'un liquide dans un canal horizontal à axe circulaire." J. Math. pures et appl., série 2 (Tome XIII), 413.

Camporeale, C., P. Perona, A. Porporato, and L. Rodolfi (2007), Hierarchy of models for meandering rivers and related morphodynamic processes, Rev. Geophys., 45, RG1001, doi:10.1029/2005RG000185.

Crosato A. (2008). "Analysis and modelling of river meandering". PhD thesis, Delft University of Technolgy, Delft, The Netherlands

de Vriend, H. J. & Geldof, H. J. (1983). "Main flow velocity in short and sharply curved river bends". Rep. 83-6, Lab. Fluid Mech., Dept. Civil Engng, Delft University of Technology.

de Vriend, H.J. and Koch, F.G. (1978). "Flow of water in a curved open channel with a fixed uneven bed". T.O.W. Rep. R657-VI/M1415-II, Delft Hydraulics Lab., Delft Univ. Techn., The Netherlands.

de Vriend, H. J., and Struiksma, N. (1984). ''Flow and bed deformation in river bends.'' River meandering, C. M. Elliot, ed., ASCE, New York, 810–828.

Dietrich, W. E., and J. D. Smith (1983). "Influence of the point bar on flow through curved channels". Water Resour. Res., 19(5), 1173– 1192.

Dietrich, W.E. and Whiting, P. (1989). "Boundary shear stress and sediment transport in river meanders of sand and gravel" in River Meandering, Water Resour. Monogr. Ser., vol. 12, edited by S. Ikeda and G. Parker, pp. 1-50, AGU, Washington, D.C.

Duarte A. (2008). "An experimental study on main flow, secondary flow and turbulence in open-channel bends with emphasis on their interaction with the outer-bank geometry.." PhD-thesis Nr 4227, Ecole Polytechnique Fédérale Lausanne, Switzerland.

Einstein, H. A. and Harder, J. A. (1954). "Velocity distribution and the boundary layer at channel bends." Trans., AGU, 35(1), 114-120.

Engelund F. (1974). "Flow and bed topography in channel bends". Journal of the Hydraulics Division, ASCE, 100(HY11), 1631-1648.

Fargue, L. (1868). "Etude sur la corrélation entre la configuration du lit et la profondeur d'eau dans les rivières à fond mobile", Annales des Ponts et Chaussées, 38, 34–92.

Ferguson, R.I., Parsons, D.R., Lane, S.N. and Hardy, R.J. (2003). "Flow in meander bends with recirculation at the inner bank". Water Resources Research 39(11): 1322.

Frothingham, K.M. and Rhoads, B.L. (2003). "Three-dimensional flow structure and channel change in an asymmetrical compound meander loop, Embarras River, Illinois". Earth Surface Processes and Landforms, 28(6), 625-644.

Hodskinson, A., and Ferguson, R. I. (1998). "Numerical modelling of separated flow in river bends: Model testing and experimental investigation of geometric controls on the extent of flow separation at the concave bank". Hydrol. Processes, 12, 1323–1338, 1998.

Hooke, R. L. (1974), Shear-stress and sediment distribution in a meander bend, Tech. Rep. UNGI RAPPORT 30, Dep. of Phys. Geogr., Univ. of Uppsala, Uppsala, Sweden.

Ikeda, S., Parker, G., and Sawai, K. (1981). "Bend theory of river meanders. Part 1. Linear development." Journal of Fluid Mechanics, 112, 363-377.

Johannesson, H. and Parker, G. (1989b). "Velocity redistribution in meandering rivers." J. Hydr. Engng, ASCE, 115(8), 1019-1039.

Kikkawa H, Ikeda S and Kitagawa A. (1976). "Flow and bed topography in curved open channles". Journal of the Hydraulics Divison – ASCE, 102(9), 1327-1342.

Leeder, M. R. and Bridge, P.H. (1975). "Flow separation in meander bends". Nature, 253, 338– 339, 1975.

Mockmore, C.A. (1943). "Flow around bends in stable channels." Transactions, ASCE, Vol. 109, 593-628 (incl. discussions).

Nelson, J. M., and J. D. Smith (1989). "Evolution and stability of erodible channel beds, in River Meandering, Water Resour. Monogr. Ser., vol. 12, edited by S. Ikeda and G. Parker, pp. 321-378, AGU, Washington, D.C.

Nezu, I., and Nakagawa, H. (1993). Turbulence in open-channel flows, Balkema, Rotterdam, The Netherlands.

Odgaard, A.J. (1986). "Meander flow model, I: Development." Journal of Hydraulic Engineering, ASCE, Vol.112(12), 1117-1136.

Odgaard, A. J., and Bergs, M. A. (1988). ''Flow processes in a curved alluvial channel.'' Water Resour. Res., 24(1), 45–56.

Pittaluga M.B., Nobile G. and Seminara G. (2009). "A nonlinear model for river meandering". Water Resources Research, 45, Article Number: W04432.

Rozovskii, I. L. (1957). Flow of water in bends of open channels, Academy of Sciences of the Ukrainian SSR, Kiev, 1957; Israel Program for Scientific Translations, Jerusalem, 1961.

Seminara G. (2006). "Meanders". Journal of fluid mechanics, 554, 271-297.

Struiksma, N., Olesen, K.W., Flokstra C. and de Vriend, H.J. (1985). "Bed deformation in curved alluvial channels." Journal of Hydraulic Research, IAHR, Vol. 23(1), 57-79.

Thomson, W. (1876). "On the origin of windings of rivers in alluvial plains, with remarks on the flow of water round bends in pipes." Proc. Royal Soc. London, 25, 5-8.

Thorne, C. R., and Hey, R. D. (1979). "Direct measurements of secondary currents at a river inflexion point." Nature, 280, 226-228.

Thorne, C. R., Zevenbergen, L. W., Pitlick, J. C., Rais, S., Bradley, J. B., and Julien, P. Y. (1985). "Direct measurement of secondary currents in a meandering sand-bed river." Nature, 315(6022), 746-747.

van Balen W., Uijttewaal WSJ and Blanckaert K. (2009a). "Large-eddy simulation of a mildly curved open-channel flow". Journal of Fluid Mechanics, 630, 413 – 442.

Van Balen W, Blanckaert K and Uijttewaal WSJ (2009). "Large-eddy simulations and xperiments of single-bend open-channel flow at different water depths". Journal of Turbulence (submitted for publication)."

Whiting, P. J., and Dietrich, W. E. (1993). "Experimental studies of bed topography and flow patterns in large-amplitude meanders. I: Observations." Water Resour. Res., 29 11 , 3605–3614.

Yen C. and B.C. Yen BC (1971). "Water surface configuration in channel bends". J. Hydraul. Div. Am. Soc. Civ. Eng., 97(HY2), 303-321.

Zeng J., Constantinescu G., Blanckaert K. and Weber L. (2008). "Flow and bathymetry in sharp open-channel bends: experiments and predictions." Water Resour. Res., 44, W09401, doi:10.1029/2007WR006303.